AMP-activated protein kinase regulates CO_2-induced alveolar epithelial dysfunction in rats and human cells by promoting Na,K-ATPase endocytosis

István Vadász, … , Werner Seeger, Jacob I. Sznajder

Research Article　**Pulmonology**

Hypercapnia (elevated CO_2 levels) occurs as a consequence of poor alveolar ventilation and impairs alveolar fluid reabsorption (AFR) by promoting Na,K-ATPase endocytosis. We studied the mechanisms regulating CO_2-induced Na,K-ATPase endocytosis in alveolar epithelial cells (AECs) and alveolar epithelial dysfunction in rats. Elevated CO_2 levels caused a rapid activation of AMP-activated protein kinase (AMPK) in AECs, a key regulator of metabolic homeostasis. Activation of AMPK was mediated by a CO_2-triggered increase in intracellular Ca^{2+} concentration and Ca^{2+}/calmodulin-dependent kinase kinase-β (CaMKK-β). Chelating intracellular Ca^{2+} or abrogating CaMKK-β function by gene silencing or chemical inhibition prevented the CO_2-induced AMPK activation in AECs. Activation of AMPK or overexpression of constitutively active AMPK was sufficient to activate PKC-ζ and promote Na,K-ATPase endocytosis. Inhibition or downregulation of AMPK via adenoviral delivery of dominant-negative AMPK-$α_1$ prevented CO_2-induced Na,K-ATPase endocytosis. The hypercapnia effects were independent of intracellular ROS. Exposure of rats to hypercapnia for up to 7 days caused a sustained decrease in AFR. Pretreatment with a β-adrenergic agonist, isoproterenol, or a cAMP analog ameliorated the hypercapnia-induced impairment of AFR. Accordingly, we provide evidence that elevated CO_2 levels are sensed by AECs and that AMPK mediates CO_2-induced Na,K-ATPase endocytosis and alveolar epithelial dysfunction, which can be prevented with β-adrenergic agonists and cAMP.

Find the latest version:

https://jci.me/29723/pdf

AMP-activated protein kinase regulates CO₂-induced alveolar epithelial dysfunction in rats and human cells by promoting Na,K-ATPase endocytosis

István Vadász,[1,2] Laura A. Dada,[1] Arturo Briva,[1,3] Humberto E. Trejo,[1] Lynn C. Welch,[1] Jiwang Chen,[1] Péter T. Tóth,[4] Emilia Lecuona,[1] Lee A. Witters,[5] Paul T. Schumacker,[6] Navdeep S. Chandel,[1] Werner Seeger,[2] and Jacob I. Sznajder[1]

[1]Division of Pulmonary and Critical Care Medicine, Feinberg School of Medicine, Northwestern University, Chicago, Illinois, USA. [2]Department of Internal Medicine, University of Giessen Lung Center, Justus Liebig University, Giessen, Germany. [3]Departamento de Fisiopatología, Facultad de Medicina, Universidad de la República, Montevideo, Uruguay. [4]Department of Pharmacological and Physiological Sciences, Feinberg School of Medicine, Northwestern University, Chicago, Illinois, USA. [5]Departments of Medicine and Biochemistry, Dartmouth Medical School, and Department of Biological Sciences, Dartmouth College, Hanover, New Hampshire, USA. [6]Department of Pediatrics, Feinberg School of Medicine, Northwestern University, Chicago, Illinois, USA.

Hypercapnia (elevated CO₂ levels) occurs as a consequence of poor alveolar ventilation and impairs alveolar fluid reabsorption (AFR) by promoting Na,K-ATPase endocytosis. We studied the mechanisms regulating CO₂-induced Na,K-ATPase endocytosis in alveolar epithelial cells (AECs) and alveolar epithelial dysfunction in rats. Elevated CO₂ levels caused a rapid activation of AMP-activated protein kinase (AMPK) in AECs, a key regulator of metabolic homeostasis. Activation of AMPK was mediated by a CO₂-triggered increase in intracellular Ca²⁺ concentration and Ca²⁺/calmodulin-dependent kinase kinase-β (CaMKK-β). Chelating intracellular Ca²⁺ or abrogating CaMKK-β function by gene silencing or chemical inhibition prevented the CO₂-induced AMPK activation in AECs. Activation of AMPK or overexpression of constitutively active AMPK was sufficient to activate PKC-ζ and promote Na,K-ATPase endocytosis. Inhibition or downregulation of AMPK via adenoviral delivery of dominant-negative AMPK-α₁ prevented CO₂-induced Na,K-ATPase endocytosis. The hypercapnia effects were independent of intracellular ROS. Exposure of rats to hypercapnia for up to 7 days caused a sustained decrease in AFR. Pretreatment with a β-adrenergic agonist, isoproterenol, or a cAMP analog ameliorated the hypercapnia-induced impairment of AFR. Accordingly, we provide evidence that elevated CO₂ levels are sensed by AECs and that AMPK mediates CO₂-induced Na,K-ATPase endocytosis and alveolar epithelial dysfunction, which can be prevented with β-adrenergic agonists and cAMP.

Introduction

Regulation of CO₂ elimination is essential for the maintenance of cellular homeostasis (1). In mammals, the lung disposes of the excess CO₂ produced by the body, and in several lung diseases the alveolar epithelium, the site of CO₂ elimination, is exposed to hypercapnia. For example, in patients with exacerbation of chronic obstructive pulmonary disease, it is not uncommon to observe pCO₂ levels of 60–80 mmHg in the arterial blood, which is associated with worse outcomes (2). Furthermore, in mechanically ventilated patients with acute lung injury and "permissive hypercapnia," pCO₂ levels are as high as 100 mmHg, and in patients with uncontrolled asthma pCO₂, levels as high as 250 mmHg have been reported (3, 4). However, whether high pCO₂ levels have a positive

or negative effect on the alveolar epithelium is still the subject of controversy (3, 5–7).
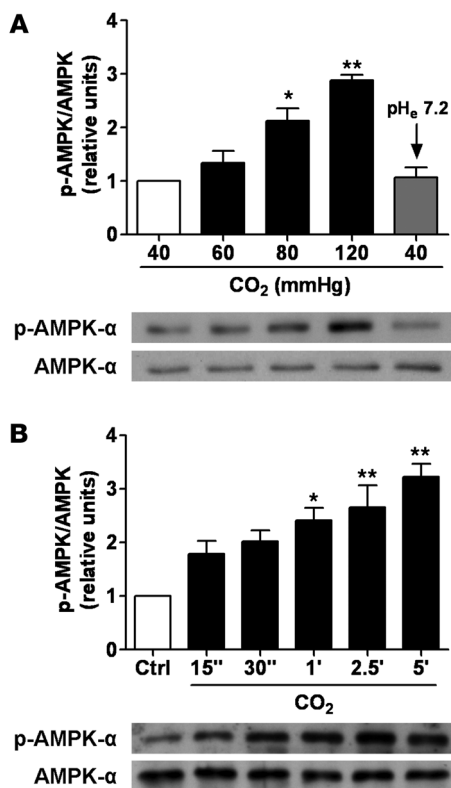
Under physiological conditions the alveolo-capillary barrier function ensures optimal gas exchange while keeping the alveoli free of edema (8, 9). Active Na⁺ transport and alveolar fluid reabsorption (AFR), major functions of the alveolar epithelium, are regulated mostly by apical Na⁺ channels and the basolateral Na,K-ATPase (8, 9). A decrease in the number of Na,K-ATPase molecules at the plasma membrane results in inhibition of Na⁺ transport, with a subsequent inhibition of alveolar fluid clearance (9–14). We and others have previously reported that the Na,K-ATPase endocytosis is triggered by the phosphorylation of its α subunit at serine 18 by PKC-ζ (10, 15). Thus regulation of the Na,K-ATPase endocytosis represents an important mechanism that maintains optimal alveolar epithelial function.

The AMP-activated protein kinase (AMPK) has been proposed as a metabolic sensor and in response to metabolic or nonmetabolic stress activates energy-generating pathways while downregulating energy-consuming events, thereby promoting cell adaptation to stress (16). AMPK is a Ser/Thr kinase that is ubiquitously expressed and highly conserved phylogenetically, with orthologs in plants and yeast (17). In the mammalian epithelium, AMPK has been reported to inhibit the epithelial Na⁺ channel (ENaC) and the cystic fibrosis

A

B

Figure 1
High CO_2 levels activate AMPK in a concentration- and time-dependent manner in ATII cells. (**A**) ATII cells were exposed to 40, 60, 80, and 120 mmHg CO_2 with an extracellular pH (pH_e) of 7.4 (white and black bars) or to 40 mmHg CO_2 with a pH_e of 7.2 (gray bar) for 5 min, and the phosphorylation of AMPK at Thr172 (pAMPK-α) and the total amount of AMPK-α was measured by Western blot analysis. Graph represents the pAMPK/AMPK ratio. Values are expressed as mean ± SEM. $n = 4$. Representative Western blots of pAMPK-α and total AMPK-α. (**B**) ATII cells were treated with 40 mmHg CO_2 (white bar) for 5 min or with 120 mmHg CO_2 for 15 s to 5 min (black bars) at a pH_e of 7.4. Graph represents the pAMPK/AMPK ratio. Values are expressed as mean ± SEM. $n = 4$. Representative Western blots of pAMPK-α and total AMPK-α. *$P < 0.05$; **$P < 0.01$.

transmembrane conductance regulator Cl⁻ channel (18, 19). Also, a recent study reported that pharmacological activation of AMPK reduces ouabain-sensitive Na⁺ transport in cultured epithelial cells, suggesting a role for AMPK in Na,K-ATPase regulation (20).

We have recently observed that exposing the alveolar epithelium to high concentrations of CO_2 impaired AFR by promoting Na,K-ATPase endocytosis from the plasma membrane of rat alveolar epithelial type II (ATII) cells (21). In the present study, we provide evidence that a short-term elevation in pCO_2 activates AMPK in a Ca^{2+}- and Ca^{2+}/calmodulin-dependent kinase kinase-β–dependent (CaMKK-β-dependent) manner in alveolar epithelial cells (AECs), leading to activation of PKC-ζ and thereby promoting Na,K-ATPase endocytosis and thus impairing fluid reabsorption, a major function of the alveolar epithelium. The inhibition of AFR was ameliorated by the β-adrenergic agonist, isoproterenol.

Results

High CO_2 levels activate AMPK in AECs. To determine whether AMPK was activated by high pCO_2 or by the hypercapnia-associated acidosis, we assessed the phosphorylation of AMPK-α subunit, which reflects the activation status of AMPK (22). Exposure of ATII cells to elevated CO_2 levels (60–120 mmHg at a pH_e of 7.4) for 5 min led to a concentration-dependent phosphorylation of AMPK at Thr172 (Figure 1A). The AMPK activation by high CO_2 levels was transient (Figure 1B) and returned to baseline values after 20 min of CO_2 exposure (data not shown). Although AMPK was not stimulated by 60 mmHg CO_2 within 5 min as with higher pCO_2, a significant stimulation of AMPK was found when ATII cells were exposed to 60 mmHg CO_2 for 10–20 min, and similarly to cells exposed to higher CO_2 levels, AMPK activity returned to baseline levels after 30 min (data not shown). In contrast, when ATII cells were exposed

to extracellular acidosis but normal CO_2 levels (pH_e 7.2 and 40 mmHg), AMPK phosphorylation was not observed (Figure 1A). Since maximal activation of AMPK was achieved at approximately 120 mmHg of CO_2 at normal pH, the subsequent cellular experiments with high CO_2 were performed under these conditions.

CO_2-induced Na,K-ATPase endocytosis is mediated by AMPK. We have recently observed that hypercapnia leads to AFR impairment and promotes Na,K-ATPase endocytosis from the plasma membrane to the intracellular compartments in AECs (21, 23). To determine whether activation of AMPK was required for the hypercapnia-induced Na,K-ATPase endocytosis, we assessed plasma membrane Na,K-ATPase protein abundance in ATII cells exposed to high CO_2 in the presence of the AMPK inhibitor compound C. Exposure of cells to 120 mmHg CO_2 decreased the plasma membrane Na,K-ATPase α_1 protein abundance by approximately 45% without affecting the total Na,K-ATPase cell pools. This effect was prevented by pretreatment of the cells with compound C (Figure 2A). Moreover, when ATII cells were infected with an adenovirus expressing a dominant-negative variant of AMPK-α_1 (DN–AMPK-α_1), endocytosis of the Na,K-ATPase α_1 subunit was prevented (in contrast to ATII cells infected with the null (Ad-null) virus; Figure 2B). To determine whether activation of AMPK was sufficient to promote Na,K-ATPase endocytosis, ATII cells were exposed to the AMPK activator 5-aminoimidazole-4-carboxamide 1-β-D-ribofuranoside (AICAR), which resulted in a decreased number of Na,K-ATPase molecules at the plasma membrane without affecting total cell Na,K-ATPase levels (Figure 2C). Furthermore, in ATII cells infected with an adenovirus expressing the constitutively active variant of AMPK-α (Ad-CA–AMPK-α), a dose-dependent reduction in the number of Na,K-ATPase molecules in the plasma membrane occurred (Figure 2D).

ROS play a key signaling role in hypoxia-induced activation of PKC-ζ, leading to Na,K-ATPase endocytosis and degradation (10, 24–26). We determined whether high CO_2 increased the production of ROS in rat ATII cells. Neither cytosolic nor mitochondrial ROS were increased by incubating AECs to elevated pCO_2 (Supplemental Figure 1, A and B; supplemental material available online with this article; doi:10.1172/JCI29723DS1), in contrast to hypoxia, in which intracellular ROS were increased (Supplemental Figure 1C). Furthermore, pretreatment of ATII cells with the ROS scavenger Eukarion 134 did not prevent the high pCO_2-induced Na,K-ATPase endocytosis but inhibited the H_2O_2-induced downregulation of Na,K-ATPase (Supplemental Figure 1D). These data suggest that ROS do not participate in the high pCO_2-induced Na,K-ATPase endocytosis.
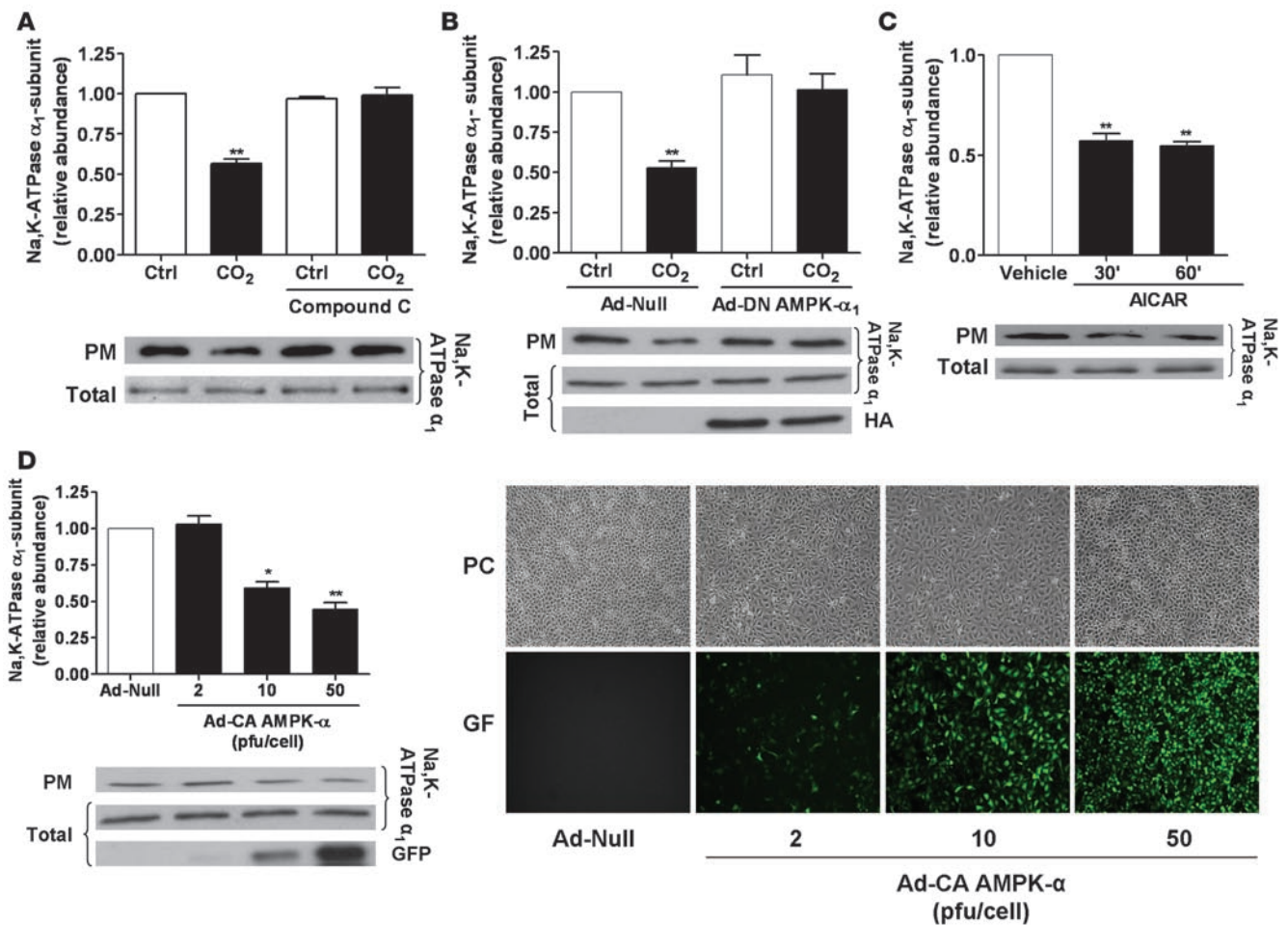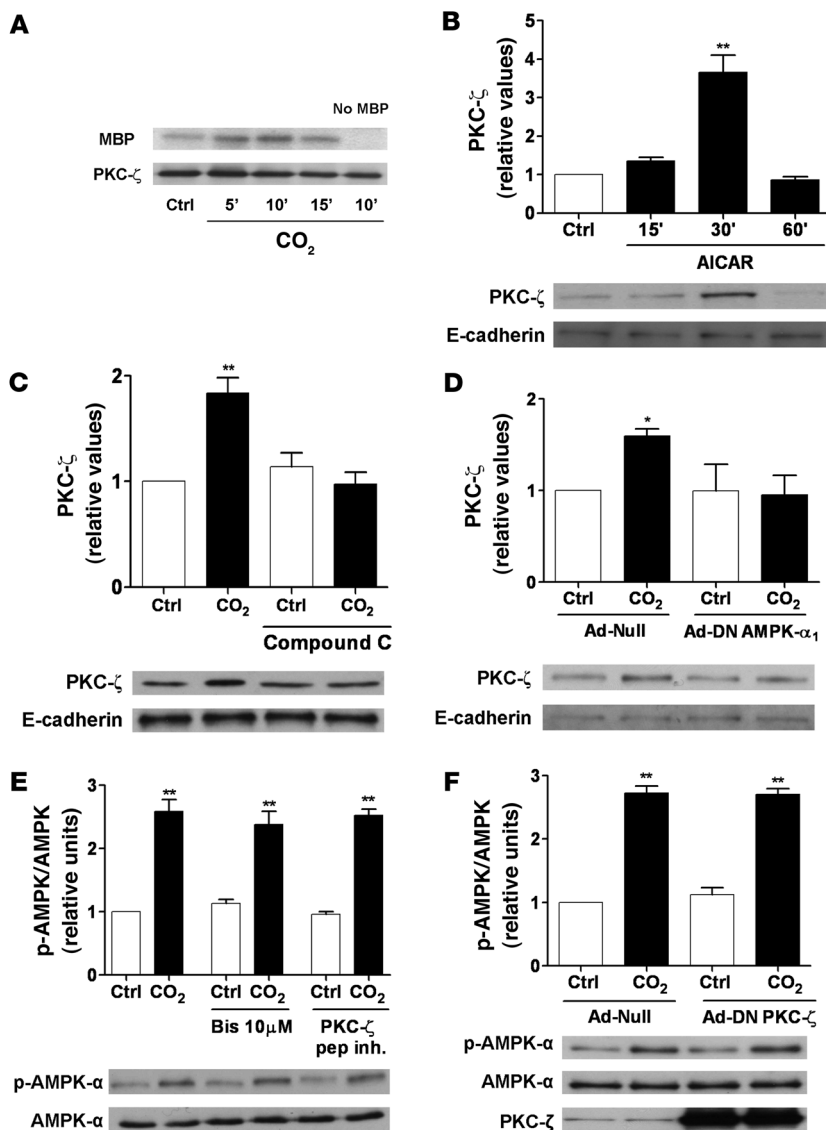
Figure 2
Activation of AMPK is both necessary and sufficient to promote Na,K-ATPase endocytosis in ATII cells. (**A**) ATII cells were exposed to 40 or 120 mmHg CO_2 for 30 min in the presence or absence of compound C (20 μM, 30 min preincubation). Na,K-ATPase at the plasma membrane was determined by biotin-streptavidin pull-down and Western blot. Representative Western blots of Na,K-ATPase-α_1 at the plasma membrane (PM) and total protein abundance are shown. (**B**) ATII cells were infected with Ad-null or HA-tagged Ad-DN–AMPK-α_1 and were exposed to 40 or 120 mmHg CO_2 for 30 min. Na,K-ATPase at the plasma membrane was determined as described above. Mean ± SEM. $n = 4$. Representative Western blots of the Na,K-ATPase-α_1 at the plasma membrane, total protein abundance, and level of HA-tagged AMPK expression are shown. (**C**) ATII cells were treated with 2 mM AICAR for 30 or 60 min or with vehicle for 60 min, and the Na,K-ATPase at the plasma membrane was determined as above. Representative Western blots of Na,K-ATPase-α_1 at the plasma membrane and total protein abundance are shown. (**D**) ATII cells were infected with Ad-null (50 pfu/cell) or a GFP-tagged Ad-CA–AMPK-α (2, 10, or 50 pfu/cell), and the amount of Na,K-ATPase was determined as described. Representative Western blots of Na,K-ATPase-α_1 at the plasma membrane, total protein abundance, and expression GFP CA-AMPK are shown. Typical phase-contrast (PC) and GFP images of infected cells are shown. Mean ± SEM. $n = 4$. *$P < 0.05$; **$P < 0.01$.

AMPK activates PKC-ζ in AECs. We and others have previously reported that PKC-ζ phosphorylation of Na,K-ATPase leads to its endocytosis (10, 13, 15), and thus we examined whether PKC-ζ was a downstream target of AMPK. Exposure of ATII cells to elevated CO_2 levels resulted in PKC-ζ activation, measured by a PKC-ζ kinase assay (Figure 3A), and translocation to the membrane fraction (Figures 3, C and D). Furthermore, the AMPK activator AICAR increased AMPK phosphorylation (data not shown) and led to PKC-ζ translocation (Figure 3B). The CO_2-induced PKC-ζ translocation was prevented by compound C, or DN–AMPK-α_1 overexpression (Figure 3, C and D). In contrast, preincubation of AECs with a high dose of bisindolylmaleimide I, with a myristoylated peptide inhibitor of PKC-ζ, or with adenovirus-mediated overexpression of DN–PKC-ζ did not prevent the CO_2-induced

AMPK activation (Figure 3, E and F), suggesting that AMPK acts upstream of PKC-ζ in the CO_2-induced signaling cascade.

Intracellular Ca^{2+} and CaMKK-β mediate the high CO_2-induced activation of AMPK. We investigated whether Ca^{2+} signaling was involved in the AMPK activation upon exposure of AECs to high CO_2 levels. Switching the perfusion of Fura-2 acetoxymethyl ester–loaded (Fura-2/AM–loaded) ATII cells from media with 40–120 mmHg pCO_2 resulted in a rapid and transient increase in intracellular Ca^{2+} ($[Ca^{2+}]_i$) concentration (Figure 4A). Chelation of intracellular Ca^{2+} with 1,2-bis(2-aminophenoxy)ethane-N,N,N′,N′-tetraacetic acid–acetoxymethyl ester (BAPTA-AM) prevented the high CO_2-induced phosphorylation of AMPK at Thr172 (Figure 4B), suggesting that intracellular Ca^{2+} was involved in the signaling cascade initiated by high pCO_2. Two upstream kinases of AMPK have been identified in

Figure 3

AMPK is upstream of PKC-ζ in the CO_2-induced signaling cascade in ATII cells. (**A**) ATII cells were exposed to 40 (Ctrl for 15 min) or 120 mmHg CO_2 for the indicated times. PKC-ζ was immunoprecipitated and incubated with MBP and $[\gamma-^{32}P]$ATP. A representative autoradiograph of the phosphorylated MBP and a Western blot of the immunoprecipitated PKC-ζ are shown. The right lane in the autoradiograph shows the result when the kinase assay was performed in the absence of MBP. $n = 4$ (**B**) ATII cells were exposed to 40 or 120 mmHg CO_2 for 5 min in the presence or absence of compound C. PKC-ζ translocation was assessed as described in Methods. Representative Western blots for PKC-ζ and the loading control E-cadherin (a membrane protein) are shown. (**C**) ATII cells were infected with Ad-null or HA-tagged Ad-DN–AMPK-α_1 and exposed to 40 or 120 mmHg CO_2 for 5 min. PKC-ζ translocation was determined as described above. Representative Western blots for PKC-ζ and E-cadherin are shown. (**D**) ATII cells were treated with 2 mM AICAR for the indicated times or with vehicle for 30 min, and translocation of PKC-ζ was determined as described above. Representative Western blots for PKC-ζ and E-cadherin are illustrated. (**E**) ATII cells were exposed to 40 or 120 mmHg CO_2 for 5 min in the presence or absence of bisindolylmaleimide I (Bis; 10 μM, 30 min preincubation) or a myristoylated peptide inhibitor of PKC-ζ (15 μM, 30 min preincubation). pAMPK-α and total AMPK-α were determined by Western blot. Graph represents the pAMPK/AMPK ratio. Representative Western blots of pAMPK-α and total AMPK-α are shown. (**F**) ATII cells were infected with Ad-null or Ad-DN–PKC-ζ and exposed to 40 or 120 mmHg CO_2 for 5 min. pAMPK-α and total AMPK-α were measured by Western blot. Graph represents the pAMPK/AMPK ratio. Representative Western blots of pAMPK-α and total AMPK-α and PKC-ζ in whole cell lysates are shown. Mean ± SEM. $n = 4$. *$P < 0.05$; **$P < 0.01$.

mammals, the protein kinase LKB1 and CaMKK-β, both of which phosphorylate AMPK at Thr172 (27). While CaMKK-β is expressed in both primary rat ATII and human epithelial A549 cells, LKB1 is found in rat ATII cells but not in A549 cells (Figure 5C), confirming previous reports that A549 cells lack LKB1 (28, 29). Exposing either cell type to high CO_2 levels resulted in similar activation of AMPK (Figure 5, A and B), suggesting a role for CaMKK-β. Furthermore, preincubation of either primary rat ATII or A549 cells with STO-609, a CaMKK-α and -β inhibitor, decreased baseline phosphorylation of AMPK at Thr172, and high pCO$_2$ did not increase AMPK phosphorylation (Figure 5, A and B). To confirm that CaMKK-β was the kinase upstream of AMPK during hypercapnia, a siRNA approach was utilized to knock down CaMKK-β expression in A549 cells. Silencing of CaMKK-β was confirmed by immunoblot, as illustrated in Figure 5D. Incubation of A549 cells with the CaMKK-β siRNA decreased the protein content by approximately 82% as compared with the control with the scrambled siRNA sequence. Similar to the effects of STO-609, baseline AMPK phosphorylation was barely detectable and remained unchanged upon exposure to high pCO$_2$ (Figure 5D).

Role of AMPK in hypercapnia-induced inhibition of AFR. To investigate whether AMPK mediated the hypercapnia-induced impairment of AFR, rat lungs were exposed to high pCO$_2$ in the presence of the AMPK inhibitor compound C or vehicle alone. Consistent with our findings in ATII cells, the CO_2-induced impairment of AFR was prevented in rat lungs pretreated with compound C (Figure 6A), without any effect on the passive movement of solutes (Figure 6B). Furthermore, when animals were infected with DN–AMPK-α_1 adenoviruses and rat lungs were exposed to high pCO$_2$ levels 7 days following adenoviral infection, the CO_2-induced impairment of AFR was also prevented without altering passive paracellular permeability for solutes (Figure 6, C and D). Histological examination of the rat lungs 7 days after infection with null or DN–AMPK-α_1 adenoviruses revealed no injury compared with sham-treated lungs, as previously reported (30, 31). In these lungs, overexpression of DN–AMPK-α_1 was observed throughout the alveolar epithelium, as assessed by immunohistochemistry and Western blot analysis of peripheral lung tissue (Figure 6, E and F).
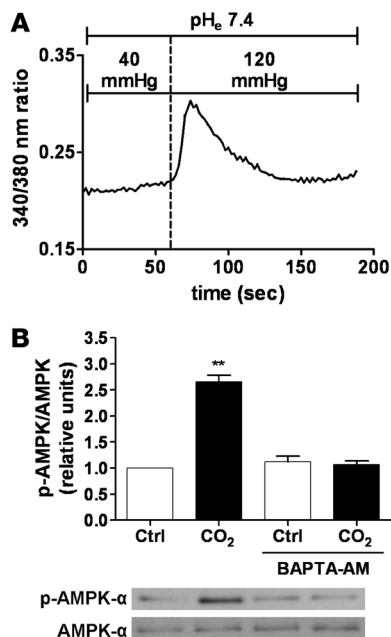
Figure 4
CO_2-induced activation of AMPK is Ca^{2+} dependent. (**A**) A representative trace of Ca^{2+} influx into ATII cells exposed to high CO_2 levels is illustrated. Fura-2–loaded cells were initially perfused with media containing 40 mmHg CO_2, and then perfusion was switched to 120 mmHg CO_2 while pH_e was maintained at 7.4. Changes in $[Ca^{2+}]_i$ are expressed as the $F340/F380$ ratio. $n = 3$. (**B**) ATII cells were exposed to 40 (white bars) or 120 (black bars) mmHg CO_2 (pH_e 7.4) for 5 min in the presence or absence of BAPTA-AM (20 μM, 20-min preincubation). pAMPK-α and total AMPK-α were determined by Western blot. Graph represents the pAMPK/AMPK ratio. Values are expressed as mean ± SEM. $n = 4$. **$P < 0.01$. Representative Western blots of pAMPK-α and total AMPK-α are shown.

Na,K-ATPase protein abundance (Figure 7C), suggesting that even though the activation of AMPK is transient, the downstream effects on Na,K-ATPase and AFR inhibition are sustained.

β-adrenergic receptor agonist and a cAMP analog ameliorate the hypercapnia-induced inhibition of AFR. To investigate whether β-adrenergic receptor and cAMP activation could prevent or overcome the hypercapnia-induced impairment of AFR, rat lungs were exposed to high pCO_2 in the presence of isoproterenol or 8-bromo-cAMP (8Br). Importantly, either pretreatment with isoproterenol or 8Br significantly ameliorated the hypercapnia-induced reduction of AFR (Figure 8, A and B) without effecting changes on passive movement of small solutes (data not shown). Moreover, when lungs were first exposed to hypercapnia and then treated with isoproterenol, there was an amelioration of the hypercapnia-induced impairment of AFR (Figure 8C).

Discussion

Here we provide evidence that AECs sense elevated CO_2 levels, resulting in very rapid activation of AMPK. The signaling cascade initiated

Long-term exposure of rats to hypercapnia impairs AFR. We measured AFR in rats maintained in an atmosphere that consisted of 10% CO_2, 21% O_2, and balanced N_2 for up to 7 days, as described in Methods. As shown in Figure 7A, AFR was markedly reduced (similar to 1 hour of ex vivo hypercapnia) after 3 and 7 days of exposure to high CO_2 levels, without deleterious effects on passive movement of small solutes across the alveolar epithelium (Figure 7B). In line with these findings, exposure of isolated ATII cells to prolonged high CO_2 resulted in a sustained decrease of plasma membrane

Figure 5
CO_2-induced activation of AMPK is mediated by CaMKK-β in ATII and A549 cells. (**A** and **B**) ATII (**A**) and A549 cells (**B**) were exposed to 40 (white bars) or 120 (black bars) mmHg CO_2 (pH_e 7.4) for 5 min in the presence or absence of STO-609 (20 μg/ml, 30 min preincubation). pAMPK-α and total AMPK-α were determined by Western blot. Graphs represent pAMPK/AMPK ratios. Values are expressed as mean ± SEM. $n = 4$. **$P < 0.01$; ###$P < 0.001$ compared with untreated cells exposed to 40 or 120 mmHg CO_2. (**C**) Expression levels of LKB1 and CaMKK-β in rat ATII and A549 cells are depicted in representative Western blots. Equal amounts of protein were loaded in each lane. Homogenates of rat kidney and rat cerebrum are shown on the left lane as positive controls for LKB1 and CaMKK-β, respectively. (**D**) A549 cells were transfected with siRNA against CaMKK-β or scrambled siRNA, and 48 h later cells were exposed to 40 (white bars) or 120 (black bars) mmHg CO_2 (pH_e 7.4) for 5 min. pAMPK-α and total AMPK-α were determined by Western blot. Graph represents the pAMPK/AMPK ratio. Values are expressed as mean ± SEM. $n = 4$. **$P < 0.01$ compared with control values; ###$P < 0.001$ compared with both 40 and 120 mmHg CO_2 controls.
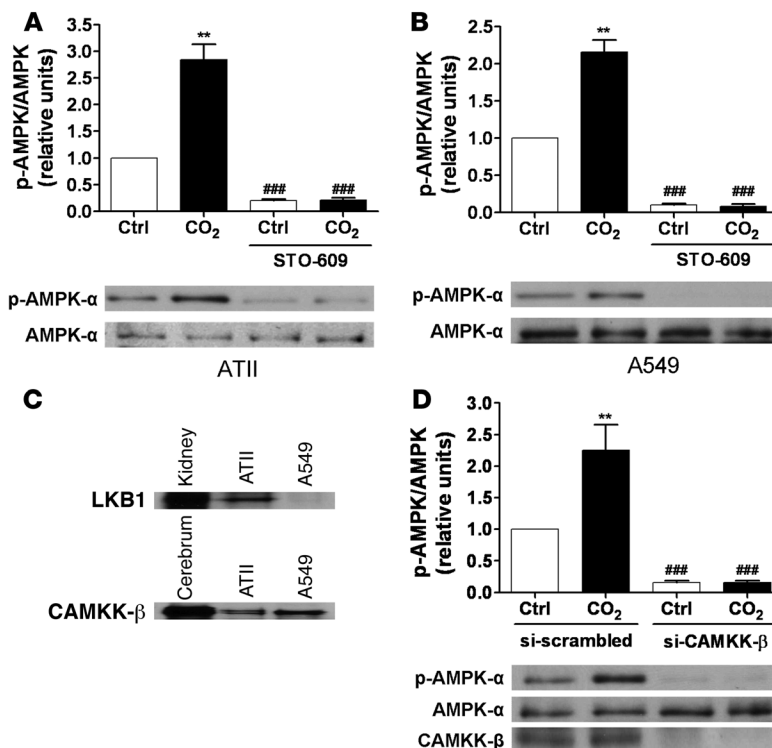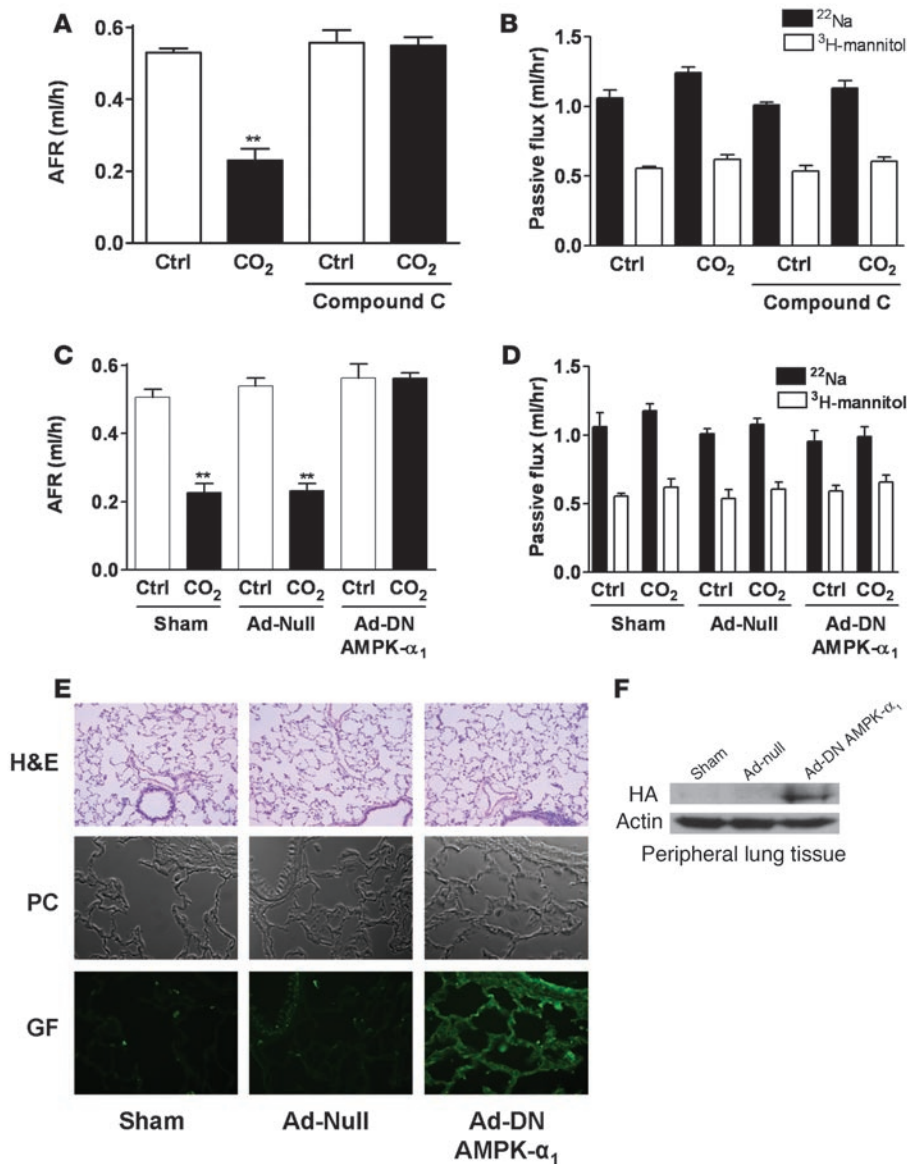
Figure 6
AMPK mediates the hypercapnia-induced impairment of AFR in rat lungs. (**A**) Isolated rat lungs were perfused for 1 h with 40 mmHg CO_2 (pH_e 7.4; white bars) or with approximately 60 mmHg CO_2 (pH_e 7.2; black bars) in the presence or absence of compound C (20 μM, 30 min preincubation), and AFR was measured as described in the supplemental material. Bars represent the mean ± SEM. $n = 5$. **$P < 0.01$. (**B**) Passive fluxes of $^{22}Na^+$ (black bars) and ^3H-mannitol (white bars) were measured as described in the supplemental material. Data represent the mean ± SEM. $n = 5$. (**C**) Isolated rat lungs from animals infected with surfactant (sham), Ad-null, or Ad-DN–AMPK-α_1 were perfused for 1 h with 40 mmHg CO_2 (pH_e 7.4; white bars) or with 60 mmHg CO_2 (pH_e 7.2; black bars), and AFR was measured as described in detail in the supplemental material. Bars represent the mean ± SEM. $n = 5$. **$P < 0.01$. (**D**) Passive fluxes of $^{22}Na^+$ (black bars) and ^3H-mannitol (white bars) were measured as described in the supplemental material. Data represent the mean ± SEM. $n = 5$. (**E**) H&E staining, phase contrast (PC), and GFP images after HA immunohistochemistry of peripheral lung tissues from sham and Ad-null– and Ad-DN–AMPK-α_1–infected rats are shown. (**F**) Representative Western blots of HA-tagged AMPK and actin (as a loading control) are shown from peripheral lung tissue homogenates from sham and Ad-null– and Ad-DN–AMPK-α_1–infected rats.

by high pCO_2 is Ca^{2+} dependent and involves CaMKK-β. Activation of AMPK leads to PKC-ζ activation, which triggers the endocytosis of the Na,K-ATPase from the plasma membrane and results in AFR inhibition, an important function of the alveolar epithelium.

The concept of CO_2 sensing was first reported in plants, which regulate CO_2 uptake from the atmosphere during photosynthesis to maintain adequate carbon import, where as a consequence of specific signaling events, stomatal opening or closing is regulated by CO_2 levels (32, 33). A CO_2 sensor has also been proposed in *Drosophila melanogaster* as well as some fungal pathogens, which are exposed to dramatically different CO_2 concentrations during infections and are able to adapt very rapidly to approximately 150-fold increases in CO_2 levels (34). Furthermore, central and peripheral chemoreception of CO_2 in mammalian neurons, such as specialized brainstem neurons and the carotid body glomus cells, were described several decades ago (reviewed in refs. 35, 36). It has also been proposed that CO_2 and pH may independently modulate the activity of carotid body glomus cells in rabbits (37). In contrast,

the mechanisms by which nonexcitable mammalian cells sense and respond to high CO_2 levels have not been elucidated.

Here we report that elevated CO_2 levels activate AMPK very rapidly and independently of pH (Figure 1, A and B). Once activated, AMPK upregulates energy-generating pathways while inhibiting energy-consuming events, thereby promoting cellular adaptation to stressful conditions (16). Since membrane transport processes consume a large proportion of cellular ATP, we reasoned that stimuli-activating AMPK may lead to the downregulation of Na,K-ATPase (38). Indeed, AMPK has been reported to inhibit the ion transporters ENaC and cystic fibrosis transmembrane conductance regulator Cl^- channel in the mammalian epithelium (18, 19). Furthermore, in a recent study, pharmacological activation of AMPK resulted in a significant decrease of amiloride- and ouabain-sensitive transepithelial Na^+ transport across H441 cell monolayers (20).We used a specific inhibitor of AMPK and a genetic approach to knock down AMPK function, both of which prevented the CO_2-induced Na,K-ATPase endocytosis (Figure 2, A and B). Importantly,
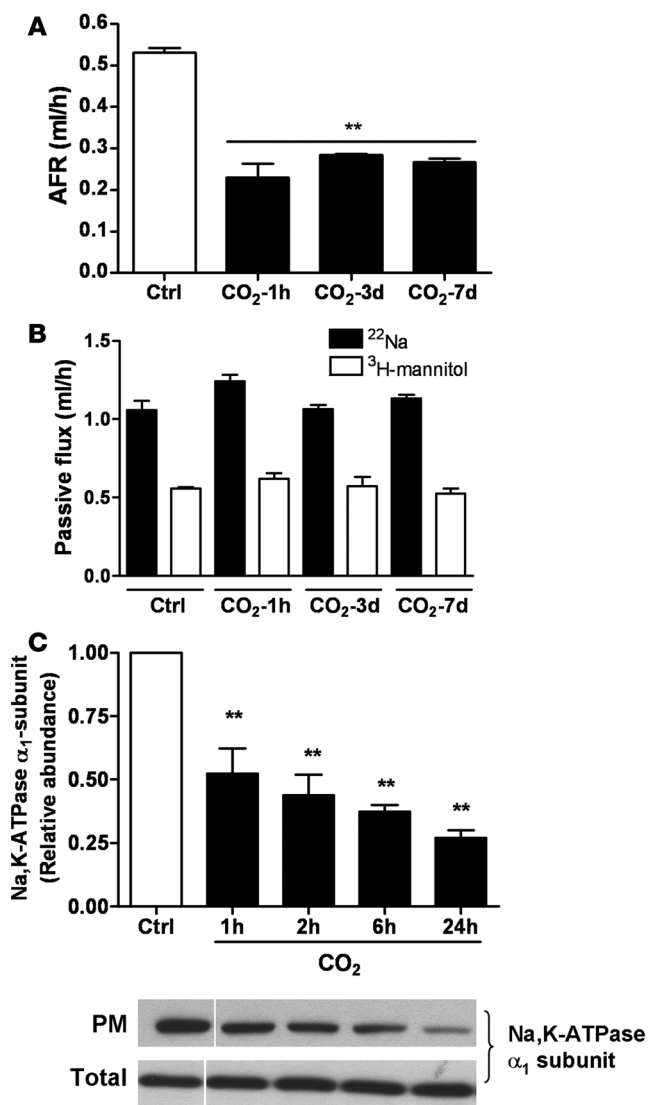
Figure 3, A and C). Furthermore, AICAR treatment or overexpression of CA–AMPK-α also resulted in Na,K-ATPase endocytosis in AECs (Figure 2, C and D), suggesting that activation of AMPK is not only necessary for the high CO_2-induced endocytosis of the Na,K-ATPase, but that it is sufficient to downregulate the Na$^+$ pump. Collectively, these data suggest that activation of AMPK by CO_2 resulted in downregulation of the Na,K-ATPase via PKC-ζ phosphorylation of the Na$^+$ pump. Interestingly, exposure of AECs to hypoxia or thrombin also promotes Na,K-ATPase endocytosis by the action of PKC-ζ (10, 13), and both have been recently proposed as potent activators of AMPK (41, 42). Thus it is possible for AMPK to be the common pathway in response to multiple stimuli that regulate the Na,K-ATPase in the alveolar epithelium.

ROS have been reported to act as intracellular messengers and activate PKC-ζ (10, 43), and recently it has been suggested that CO_2 may interact with ROS (44). However, we did not observe changes in intracellular ROS, nor in the cytosolic or mitochondrial compartments when AECs were exposed to high CO_2 levels. Furthermore, pretreatment of cells with the antioxidant Eukarion 134 had no effect on the CO_2-induced endocytosis of Na,K-ATPase from the plasma membrane. Thus we reason that the CO_2-induced and PKC-ζ-mediated effects on the Na,K-ATPase were independent of ROS, which is distinct from previously reported stimuli that impair Na,K-ATPase function via PKC-ζ phosphorylation in the alveolar epithelium (10, 13, 45).

In mammals, LKB1 and CaMKK-β have been identified as upstream kinases of AMPK, since both kinases can phosphorylate Thr172 and thus activate AMPK (22, 27, 46–49). While phosphorylation of Thr172 by LKB1 requires an increase in AMP (50, 51), the phosphorylation of Thr172 by CaMKK-β is independent of AMP levels and is triggered by a rise in intracellular Ca^{2+} (29, 42, 47, 48, 52). We found that exposing AECs to high pCO$_2$ initiated a rapid and transient influx of Ca^{2+} into the cells (Figure 4A) and that AMPK activation by high CO_2 concentrations was prevented by the intracellular Ca^{2+}-chelating agent, BAPTA-AM (Figure 4B), suggesting that the CO_2-induced signaling pathway was dependent upon intracellular Ca^{2+}. Since CaMKK-β–mediated stimulation of AMPK required an increase in intracellular Ca^{2+} levels, we hypothesized that CaMKK-β may be the upstream kinase induced by high pCO$_2$. Indeed, the CaMKK inhibitor STO-609 decreased the baseline AMPK activity and prevented activation of the AMPK upon high CO_2 exposure in ATII cells (Figure 5A). Moreover, identical experiments performed in human epithelial

the overexpression of DN–AMPK-α in the alveolar epithelium prevented the hypercapnia-induced impairment of AFR (Figure 6). Although we cannot exclude that the AMPK-α$_2$ subunit may also participate in the CO_2-induced signaling pathway, it appears that the AMPK-α$_1$ subunit plays a prominent role in the signaling initiated by high pCO$_2$ levels.

Since we have previously described that the endocytosis of the Na,K-ATPase requires phosphorylation of the Na$^+$ pump at Ser18 by PKC-ζ (10, 21), we hypothesized that PKC-ζ might be regulated by AMPK. CO_2 caused time-dependent PKC-ζ activation, which was prevented by pharmacological inhibitors or genetic modulation of AMPK activity (see Figure 3). In contrast, inhibition of PKC-ζ had no effect on AMPK activation upon CO_2 stimulation (Figure 3, E and F). We also found that treatment of ATII cells with AICAR, a chemical activator of AMPK, resulted in PKC-ζ activation (Figure 3B), similar to the effects of high pCO$_2$. AICAR is taken up by cells, where it is metabolized to AICA-ribotide, which mimics the effect of AMP on AMPK (39, 40), and therefore, it is not surprising that the AICAR-induced activation of PKC-ζ occurred later (30 min; Figure 3B) than activation of PKC-ζ by CO_2 (5 min;
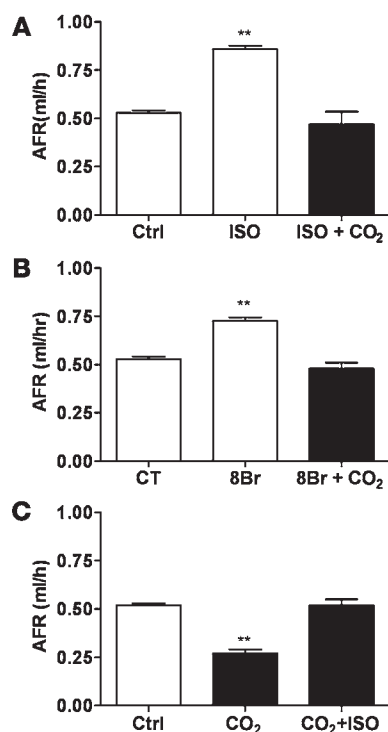
Figure 8
The hypercapnia-induced impairment of AFR in rat lung is amelio-rated by isoproterenol and 8Br. (**A**) Isolated rat lungs were perfused for 1 h with 40 mmHg CO_2 in the absence (Ctrl) and then for 1 h in the presence of isoproterenol (1 μM, ISO), after which perfusion was switched to approximately 60 mmHg CO_2 in the continuous presence of isoproterenol, and AFR was measured as described in the supple-mental material. Bars represent the mean ± SEM. $n = 5$. **$P < 0.01$. (**B**) Isolated rat lungs were perfused for 1 h with 40 mmHg CO_2 in the absence and then for 1 h in the presence of 8Br (100 μM), after which perfusion was switched to approximately 60 mmHg CO_2 in the con-tinuous presence of 8Br, and AFR was measured as above. Bars represent the mean ± SEM. $n = 5$. **$P < 0.01$. (**C**) Isolated rat lungs were perfused for 1 h with 40 mmHg CO_2, and then perfusion was switched to approximately 60 mmHg for 1 h in the absence and then for 1 h in the presence of isoproterenol (1 μM). AFR was mea-sured as described in the supplemental material. Bars represent the mean ± SEM. $n = 5$. **$P < 0.01$.

A549 cells, which lack LKB1 (28, 29) but express CaMKK-β, and in ATII cells, which express both kinases, revealed a comparable acti-vation of AMPK by CO_2. Similarly, pretreatment with the CaMKK inhibitor prevented AMPK activation by high CO_2 in A549 cells (Figure 5B), and when these cells were transfected with siRNA to silence CaMKK-β, both baseline and high CO_2-induced activity of AMPK were nearly undetectable (Figure 5D). It has been well established that activation of AMPK is transient in CaMKK-β–mediated responses and returns to baseline levels when the intracellular Ca^{2+} levels fall (42, 47, 53), while AMPK activation via LKB1 (which appears to be constitutively active) is rather sustained (46). Consistent with other CaMKK-β–dependent responses, activation of AMPK by elevated CO_2 levels was also rapid and transient. These data suggest that the high CO_2-induced activa-tion of AMPK was mediated by CaMKK-β independently of LKB1 signaling. Interestingly, the CO_2-sensitive brainstem neurons and

glomus cells also adapt to hypercapnia via an increase in $[Ca^{2+}]_i$ (37, 54, 55), thus it is possible that CaMKK-β and AMPK are also involved in CO_2 sensing in excitable cells.

We present evidence that in AECs, high pCO_2 levels increase the $[Ca^{2+}]_i$, which results in activation of CaMKK-β, leading to AMPK activation. The elevation of intracellular Ca^{2+} levels can regulate a broad spectrum of cellular processes through precise spatial and temporal regulation of the Ca^{2+} signal (56–58). There are many examples of different cell types that utilize distinct signaling mechanisms to increase intracellular Ca^{2+} in a stimu-lus-specific manner (58). For example, in fetal AECs, elevation of intracellular Ca^{2+} by β-adrenergic receptor activation stimulation leads to the activation of the amiloride-sensitive, nonselective cation channel, which contributes to the clearance of lung fluid (59, 60), whereas, as we demonstrate in this manuscript, during hypercapnia, increased $[Ca^{2+}]_i$ activates CaMKK-β and AMPK, leading to Na,K-ATPase downregulation and inhibition of AFR. These contrasting effects of Ca^{2+} signaling might be attributed to alternative sources of Ca^{2+} and/or the compartmentalized loca-tion and strength of the signal. The source of Ca^{2+} in the high pCO_2 response warrants further studies.

An important function of the alveolar epithelium is to maintain optimal gas exchange. Thus to keep the alveoli "dry" and exchange O_2 and CO_2, AECs reabsorb the fluid that moves into the airspaces. This is achieved largely by the activity of ENaC and the Na,K-ATPase, contributing to active Na^+ transport across the alveolar epithelium (8, 9). We observed that hypercapnia impaired AFR by inhibiting Na,K-ATPase function. Importantly, hypoxia also diminishes AFR by downregulating both ENaC (61, 62) and Na,K-ATPase (10, 63). Thus both hypercapnia and hypoxia, the 2 key components of acute respiratory failure, have deleterious effects on alveolar epithelial function and thereby might impair the reso-lution of pulmonary edema and thus the recovery of patients with acute lung injury (64). Importantly, both the β-adrenergic agonist isoproterenol and the cAMP analog 8Br ameliorated the deleteri-ous effects of hypercapnia on AFR. Indeed, β-adrenergic receptor agonists and cAMP are emerging as exciting new avenues for the management of patients with acute lung injury (65). These agents have been shown to overcome or prevent the effects of experimen-tal acid-induced lung injury (66), hydrostatic edema (67), ventila-tor-associated lung injury (68), and hypoxia (11, 61, 62).

We have also performed studies to address the effects of pro-longed hypercapnia on alveolar epithelial function, as a prolonged exposure would more accurately mimic clinical situations. We have found that both short- and long-term hypercapnia (at levels simi-lar to those observed in patients with chronic obstructive pulmo-nary disease and permissive hypercapnia) resulted in comparable alveolar epithelial dysfunction (see Figure 7). These data suggest that hypercapnia may contribute to disease states in patients with increased CO_2 levels.

In summary, we provide evidence that AECs sense elevated CO_2 levels, initiating an intracellular Ca^{2+}–dependent signaling path-way that involves the activation of CaMKK-β, AMPK, and PKC-ζ, triggering the endocytosis of Na,K-ATPase molecules and thus impairing AFR, an essential function of the alveolar epithelium. These results are of particular pathophysiological significance, given that the mammalian alveolar epithelium is the site of CO_2 elimination. Further studies are warranted to elucidate the mecha-nisms by which the alveolar epithelium is affected by hypercapnia in patients with lung disease.

Methods

Reagents. All cell culture reagents were from Mediatech Inc. $^{22}Na^+$ was from GE Healthcare. ^3H-mannitol was from PerkinElmer. The myristoylated PKC-ζ peptide inhibitor was from Biomol International. BAPTA-AM was from Sigma-Aldrich. siRNA against CaMKK-β was from Qiagen. Lipofectamine RNAiMAX and Opti-MEM I reduced serum medium were from Invitrogen. The inhibitor of CaMKK, STO-609 (69), was from Calbiochem. A monoclonal antibody directed against the Na,K-ATPase α_1 subunit (clone 464.6) and myelin basic protein (MBP) were from Upstate Biotechnology. Antibodies against PKC-ζ, GFP, and LKB1 (Ley37D/G6) were from Santa Cruz Biotechnology Inc. All other primary antibodies were from Cell Signaling. Secondary goat anti-mouse HRP was from Bio-Rad, and goat anti-rabbit HRP was from Cell Signaling. All other chemicals were purchased from Calbiochem.

Animals. Pathogen-free adult male Sprague-Dawley rats were from Harlan. Animals were provided with food and water ad libitum, were maintained on a 12-hour light/12-hour dark cycle and were handled according to NIH guidelines and the Northwestern University Animal Care and Use Committee–approved experimental protocols.

Isolation and culture of AECs. Type II AECs were isolated from the lungs of Sprague-Dawley rats weighing 200–225 g, as previously described (31). The day of isolation and plating was designated culture day 0. All experiments were conducted on days 2 or 3. A549 cells (ATCC, CCL 185) were grown in DMEM supplemented with 10% fetal bovine serum and 100 U/ml penicillin, 100 μg/ml streptomycin. Experiments were performed on subconfluent monolayers of A549 cells. All cells were incubated in a humidified atmosphere of 5% CO_2/95% air at 37°C.

CO_2 media and CO_2 exposure. For the different experimental conditions, initial solutions were prepared with DMEM-Ham's F-12 medium-Tris base (3:1:0.5) containing 10% fetal bovine serum with 100 U/ml penicillin, and 100 μg/ml streptomycin. The buffering capacity of the media was modified by changing its initial pH with Tris base in order to obtain a pH of 7.4 at the various CO_2 levels (pCO_2 of 40, 60, 80, and 120 mmHg). In some experiments, modeling extracellular acidosis, an initial pH of 6.8 was used, resulting in a final pH of 7.2 and a pCO_2 of 40 mmHg. The desired CO_2 and pH levels were achieved by equilibrating the media overnight in a humidified chamber (C-Chamber; Biospherix Ltd.). The C-Chamber's atmosphere was controlled with a PRO-CO_2 Carbon Dioxide controller (Biospherix). In this chamber, cells were exposed to the desired pCO_2 while maintaining 21% O_2 balanced with N_2. Prior to and after CO_2 exposure, pH, pCO_2, and pO_2 levels in the media were measured using a Stat Profile pHOx blood gas analyzer (Nova Biomedical). Experiments were started by replacing culture media with the CO_2-equilibrated media and incubating in the C-Chamber for the desired time. Normoxic conditions were consistent over the course of all experiments.

Adenoviral infection of ATII cells. Day 2 ATII cells, plated on 60-mm cell culture dishes were incubated with Ad-null (20 or 50 pfu/cell) or with an Ad-DN kinase-dead (K45R) variant of the AMPK-α_1 subunit (Ad-DN–AMPK-α_1; 20 pfu/cell) (70) or with a constitutively active AMPK-α variant (Ad-CA–AMPK-α), in which Thr172 was substituted with aspartate in the truncated 1-312 AMPK-α subunit (a generous gift from Kenneth Walsh, Boston University, Boston, Massachusetts, USA; 2, 10, or 50 pfu/cell) (71) or with an adenovirus expressing a DN PKC-ζ (Ad-DN–PKC-ζ; Cell Biolabs) for 2–4 h in 500 μl DMEM. After the 2- to 4-h incubation period, 1.5 ml of DMEM supplemented with 10% fetal bovine serum, 100 U/ml penicillin, and 100 μg/ml streptomycin was added to the cell culture plates, and experiments were performed 24 h later.

Transfection of A549 cells with siRNA. A549 cells were plated in 60-mm cell culture dishes and transfected with 60 pmol siRNA duplex using Lipofectamine RNAiMAX (Invitrogen) as recommended by the manufacturer,

and experiments were performed 48 h later. The following siRNA were applied to target CaMKK-β: 5′-CGAUCGUCAUCUCUGGGUUAdTdT-3′ and 5′-UAACCAGAGAUGACGAUCG-3′ (sense and antisense, respectively). As a nonsilencing negative control, 5′-UUCUCCGAACGUGUCACGUdT-dT-3′ (sense) and 5′-ACGUGACACGUUCGGAGAAdTdT-3′ (antisense) were applied (all from Qiagen).

Biotinylation of cell surface proteins. Cells were labeled for 20 min using 1 mg/ml EZ-link NHS-SS-biotin (Pierce Biotechnology), and surface proteins were pulled down with streptavidin-Sepharose beads (Pierce Biochemical), as previously described (10, 72, 73). Proteins were analyzed by SDS-PAGE and Western blot.

Western blot analysis. Protein concentration was quantified by Bradford assay (Bio-Rad), and proteins were resolved in 10%–15% polyacrylamide gels. Thereafter, proteins were transferred to nitrocellulose membranes (Optitran; Schleider & Schuell) using a semi-dry transfer apparatus (Bio-Rad). Incubation with specific antibodies was performed overnight at 4°C. Blots were developed with a chemiluminescence detection kit (Perkin-Elmer), as recommended by the manufacturer. The bands were quantified by densitometric scanning (Image J 1.29X; NIH).

Cell fractionation. Cells were exposed to 40 or 120 mmHg CO_2 at 37°C for 5 min, placed on ice, and washed twice with ice-cold PBS. Cells were scraped in homogenization buffer (1 mM EDTA, 1 mM EGTA, 10 mM Tris-HCl, pH 7.5, 1 μg/ml leupeptin, 100 μg/ml TPCK, and 1 mM PMSF) and homogenized. Homogenates were centrifuged at 500 g to discard nuclei and debris, and the supernatant was centrifuged at 100,000 g for 1 h at 4°C. The pellet containing the crude membrane fraction was resuspended in homogenization buffer supplemented with 1% Triton X-100 and centrifuged at 100,000 g for 30 min at 4°C. The supernatant was designated the 1% Triton X-100–soluble membrane fraction (74).

PKC-ζ kinase assay. PKC-ζ activity was measured as previously described (75). Briefly, cell lysates were obtained after exposure to CO_2, and PKC-ζ was immunoprecipitated by incubating overnight approximately 500 μg protein with 5 μl PKC-ζ antibody (Santa Cruz Biotechnology Inc.). Immunocomplexes were pulled down with 50 μl Protein A/G agarose beads and then washed in lysis buffer. The immunoprecipitates were incubated with 2 μg MBP, 10 μCi [γ-^{32}P]–ATP, 100 μM ATP for 30 min at 30°C in 35 mM Tris, pH 7.5, 10 mM $MgCl_2$, 5 mM EGTA, 1 mM $CaCl_2$, and 10 mM β-glycerolphosphate. The reactions were stopped by adding SDS sample buffer and boiling the samples. The proteins were separated by SDS-PAGE, and radiolabeled MBP was detected by autoradiography.

Measurement of intracellular Ca^{2+}. The ATII cells were loaded with Fura-2/AM (Invitrogen), which was used as a fluorescence indicator of intracellular-free Ca^{2+} levels. Dye loading was performed in the standard buffer solution at pH 7.3 and supplemented with 2 μM Fura-2/AM. Cells were incubated with the dye-loading solution for 30 min at room temperature in the dark and further incubated for 30 min at room temperature to complete deesterification of the dye. Free Ca^{2+} concentrations were measured by digital video microfluorimetry using an intensified CCD camera coupled to the microscope. Fura-2 dye was excited through 340-nm and 380-nm interference filters housed in a computer-controlled filter wheel. The fluorescence emitted was collected at 510 nm. The data acquisition of Fura-2 videoimaging was obtained using a Nikon TE2000 (Nikon Instruments Inc.) equipped with an environmental control system chamber (FCS2 system; Bioptechs Inc.) and a Plan Fluor 40× 1.30 oil objective (Nikon Instruments Inc). During imaging, the chamber was perfused with the specific culture media described above equilibrated at 40 or 120 mmHg CO_2 (pH$_e$ 7.4). Images were collected with a Cascade camera TC285 EMCCD with on-chip multiplication gain (Photometrics) driven by MetaFluor Software (Molecular Devices Corp.). For all the experiments, exposure time was 100 ms, and to decrease phototoxic effects, 0.5 neutral filter was used. Changes in [Ca^{2+}]$_i$ were expressed using

conventional $F340/F380$ ratio (the ratio of the Fura-2 fluorescence intensities measured at wavelengths of 340 nm and 380 nm).

Adenoviral infection of rats. Rats were anesthetized with 40 mg/kg nembutal i.p. and orally intubated with a 14-gauge plastic catheter prior to adenoviral infection. Three experimental groups were studied: sham-surfactant ($n = 5$), Ad-null ($n = 5$), and Ad-DN–AMPK-α_1 ($n = 5$). A mixture of adenovirus (4×10^9 PFU) in a 50% surfactant (Forest Laboratories Inc.), 50% dialysis buffer vehicle was administered in 4 aliquots of 250 μl. Rats were rotated 90° between instillations given at 5-min intervals. Immediately before instillation, a forced exhalation was achieved by circumferential compression of the thorax (31). Compression was relinquished after endotracheal instillation of 250 μl of virus/vehicle followed by 500 μl of air. Rats were allowed to recover before extubation. Infected animals were maintained in separate isolator cages for 7 days prior to conducting experiments, as described previously (30, 31).

Long-term exposure of rats to hypercapnia. Pathogen-free male Sprague-Dawley rats (300–325 g) were maintained in a continuously monitored Biospherix A Chamber for 3 or 7 days. The chamber atmosphere was controlled with a ProOx model C-21 O_2/CO_2 controller combination (Biospherix) at 10% CO_2, 21% O_2, with a temperature of 23–26°C and a relative humidity between 40% and 50%, and animals were allowed access to food and water ad libitum. No animals developed appreciable distress and were monitored visually by the investigators 3 times daily (at 8 am, 12 pm, and 7 pm). The arterial pCO_2 in the animals exposed to CO_2 for 7 days was 74 ± 6 mmHg. All experiments were approved by the Northwestern University Animal Care and Use Committee.

Isolated perfused rat lung model. The isolated lung preparation has been previously described in detail (12). A brief description of this methodology is provided in Supplemental Data. During hypercapnia, pCO_2 was 69 ± 4 mmHg, resulting in a pH of 7.26 ± 0.02. The pO_2 was constant in all experimental groups (160 ± 4 mmHg).

Immunohistochemistry. Longitudinal sections from fixed lungs were embedded in paraffin for immunohistochemical analysis. Primary antibody directed against the HA epitope (1:500 dilution) was added for 1 h at room temperature. Sections were washed with PBS prior to the addition of goat anti-mouse secondary antibody. Immunodetection was accomplished by 3,3′-diaminobenzidine staining for immunoperoxidase activity (Vector Elite ABC kit; Vector Laboratories). Sections were photographed using a digital photomicroscopy system (Spot II; Diagnostic Instruments).

Statistics. Data are expressed as mean ± SEM. Data were compared using analysis of variance adjusted for multiple comparisons with the Dunnet test. When comparisons were performed between 2 groups, significance was evaluated by Student's *t* test. A P value of less than 0.05 was considered significant.

Address correspondence to: Jacob I. Sznajder, Pulmonary and Critical Care Medicine, 240 E. Huron, McGaw M-300, Northwestern University, Feinberg School of Medicine, Chicago, Illinois 60611, USA. Phone: (312) 908-7737; Fax: (312) 908-4650; E-mail: j-sznajder@northwestern.edu.

1. Putnam, R.W., Filosa, J.A., and Ritucci, N.A. 2004. Cellular mechanisms involved in CO(2) and acid signaling in chemosensitive neurons. *Am. J. Physiol. Cell Physiol.* **287**:C1493–C1526.
2. Connors, A.F., Jr., et al. 1996. Outcomes following acute exacerbation of severe chronic obstructive lung disease. The SUPPORT investigators (Study to Understand Prognoses and Preferences for Outcomes and Risks of Treatments). *Am. J. Respir. Crit. Care Med.* **154**:959–967.
3. Laffey, J.G., and Kavanagh, B.P. 1999. Carbon dioxide and the critically ill — too little of a good thing? *Lancet.* **354**:1283–1286.
4. Mutlu, G.M., Factor, P., Schwartz, D.E., and Sznajder, J.I. 2002. Severe status asthmaticus: management with permissive hypercapnia and inhalation anesthesia. *Crit. Care Med.* **30**:477–480.
5. Lang, J.D., et al. 2005. Hypercapnia via reduced rate and tidal volume contributes to lipopolysaccharide-induced lung injury. *Am. J. Respir. Crit. Care Med.* **171**:147–157.
6. Doerr, C.H., et al. 2005. Hypercapnic acidosis impairs plasma membrane wound resealing in ventilator-injured lungs. *Am. J. Respir. Crit. Care Med.* **171**:1371–1377.
7. Laffey, J.G., et al. 2000. Therapeutic hypercapnia reduces pulmonary and systemic injury following in vivo lung reperfusion. *Am. J. Respir. Crit. Care Med.* **162**:2287–2294.
8. Matthay, M.A., Folkesson, H.G., and Clerici, C. 2002. Lung epithelial fluid transport and the resolution of pulmonary edema. *Physiol. Rev.* **82**:569–600.
9. Vadasz, I., Raviv, S., and Sznajder, J.I. 2007. Alveolar epithelium and Na,K-ATPase in acute lung injury. *Intensive Care Med.* **33**:1243–1251.
10. Dada, L.A., et al. 2003. Hypoxia-induced endocytosis of Na,K-ATPase in alveolar epithelial cells is mediated by mitochondrial reactive oxygen species and PKC-zeta. *J. Clin. Invest.* **111**:1057–1064.
11. Litvan, J., et al. 2006. Beta-adrenergic receptor stimulation and adenoviral overexpression of superoxide dismutase prevent the hypoxia-mediated decrease in Na,K-ATPase and alveolar fluid reabsorption. *J. Biol. Chem.* **281**:19892–19898.
12. Saldias, F.J., et al. 2001. Alveolar fluid reabsorption is impaired by increased left atrial pressures in rats. *Am. J. Physiol. Lung Cell Mol. Physiol.* **281**:L591–L597.
13. Vadasz, I., et al. 2005. Thrombin impairs alveolar fluid clearance by promoting endocytosis of Na+,K+-ATPase. *Am. J. Respir. Cell Mol. Biol.* **33**:343–354.
14. Morty, R.E., Eickelberg, O., and Seeger, W. 2007. Alveolar fluid clearance in acute lung injury: what have we learnt from animal models and clinical studies? *Intensive Care Med.* **33**:1229–1240.
15. Chibalin, A.V., et al. 1998. Phosphorylation of the catalytic alpha-subunit constitutes a triggering signal for Na+,K+-ATPase endocytosis. *J. Biol. Chem.* **273**:8814–8819.
16. Kemp, B.E., et al. 2003. AMP-activated protein kinase, super metabolic regulator. *Biochem. Soc. Trans.* **31**:162–168.
17. Hardie, D.G., Carling, D., and Carlson, M. 1998. The AMP-activated/SNF1 protein kinase subfamily: metabolic sensors of the eukaryotic cell? *Annu. Rev. Biochem.* **67**:821–855.
18. Bhalla, V., et al. 2006. AMP-activated kinase inhibits the epithelial Na+ channel through functional regulation of the ubiquitin ligase Nedd4-2. *J. Biol. Chem.* **281**:26159–26169.
19. Hallows, K.R., Raghuram, V., Kemp, B.E., Witters, L.A., and Foskett, J.K. 2000. Inhibition of cystic fibrosis transmembrane conductance regulator by novel interaction with the metabolic sensor AMP-activated protein kinase. *J. Clin. Invest.* **105**:1711–1721.
20. Woollhead, A.M., Scott, J.W., Hardie, D.G., and Baines, D.L. 2005. Phenformin and 5-aminoimidazole-4-carboxamide-1-beta-D-ribofuranoside (AICAR) activation of AMP-activated protein kinase inhibits transepithelial Na+ transport across H441 lung cells. *J. Physiol.* **566**:781–792.
21. Briva, A., et al. 2007. High CO2 levels impair alveolar epithelial function independently of pH. *PLoS ONE.* **2**:e1238.
22. Hawley, S.A., et al. 1996. Characterization of the AMP-activated protein kinase kinase from rat liver and identification of threonine 172 as the major site at which it phosphorylates AMP-activated protein kinase. *J. Biol. Chem.* **271**:27879–27887.
23. Chen, J., Lecuona, E., Briva, A., Welch, L.C., and Sznajder, J.I. 2008. Carbonic anhydrase II and alveolar fluid reabsorption during hypercapnia. *Am. J. Respir. Cell Mol. Biol.* **38**:32–37.
24. Comellas, A.P., et al. 2006. Hypoxia-mediated degradation of Na,K-ATPase via mitochondrial reactive oxygen species and the ubiquitin-conjugating system. *Circ. Res.* **98**:1314–1322.
25. Dada, L.A., Novoa, E., Lecuona, E., Sun, H., and Sznajder, J.I. 2007. Role of the small GTPase RhoA in the hypoxia-induced decrease of plasma membrane Na,K-ATPase in A549 cells. *J. Cell Sci.* **120**:2214–2222.
26. Jain, M., and Sznajder, J.I. 2005. Effects of hypoxia on the alveolar epithelium. *Proc. Am. Thorac. Soc.* **2**:202–205.
27. Witters, L.A., Kemp, B.E., and Means, A.R. 2006. Chutes and Ladders: the search for protein kinases that act on AMPK. *Trends Biochem. Sci.* **31**:13–16.
28. Sanchez-Cespedes, M., et al. 2002. Inactivation of LKB1/STK11 is a common event in adenocarcino-

mas of the lung. *Cancer Res.* **62**:3659–3662.

29. Hurley, R.L., et al. 2005. The Ca2+/calmodulin-dependent protein kinase kinases are AMP-activated protein kinase kinases. *J. Biol. Chem.* **280**:29060–29066.

30. Factor, P., et al. 1998. Augmentation of lung liquid clearance via adenovirus-mediated transfer of a Na,K-ATPase beta1 subunit gene. *J. Clin. Invest.* **102**:1421–1430.

31. Ridge, K.M., et al. 2003. Alveolar type 1 cells express the alpha2 Na,K-ATPase, which contributes to lung liquid clearance. *Circ. Res.* **92**:453–460.

32. Mansfield, T.A., Hetherington, A.M., and Atkinson, C.J. 1990. Some current aspects of stomatal physiology. *Annu. Rev. Plant Physiol. Plant Mol. Biol.* **41**:55–75.

33. Young, J.J., et al. 2006. CO(2) signaling in guard cells: calcium sensitivity response modulation, a Ca(2+)-independent phase, and CO(2) insensitivity of the gca2 mutant. *Proc. Natl. Acad. Sci. U. S. A.* **103**:7506–7511.

34. Bahn, Y.S., and Muhlschlegel, F.A. 2006. CO2 sensing in fungi and beyond. *Curr. Opin. Microbiol.* **9**:572–578.

35. Gourine, A.V. 2005. On the peripheral and central chemoreception and control of breathing: an emerging role of ATP. *J. Physiol.* **568**:715–724.

36. Lahiri, S., and Forster, R.E., 2nd. 2003. CO2/H(+) sensing: peripheral and central chemoreception. *Int. J. Biochem. Cell Biol.* **35**:1413–1435.

37. Summers, B.A., Overholt, J.L., and Prabhakar, N.R. 2002. CO(2) and pH independently modulate L-type Ca(2+) current in rabbit carotid body glomus cells. *J. Neurophysiol.* **88**:604–612.

38. Hallows, K.R. 2005. Emerging role of AMP-activated protein kinase in coupling membrane transport to cellular metabolism. *Curr. Opin. Nephrol. Hypertens.* **14**:464–471.

39. Corton, J.M., Gillespie, J.G., Hawley, S.A., and Hardie, D.G. 1995. 5-aminoimidazole-4-carboxamide ribonucleoside. A specific method for activating AMP-activated protein kinase in intact cells? *Eur. J. Biochem.* **229**:558–565.

40. Lizcano, J.M., et al. 2004. LKB1 is a master kinase that activates 13 kinases of the AMPK subfamily, including MARK/PAR-1. *EMBO J.* **23**:833–843.

41. Mu, J., Brozinick, J.T., Jr., Valladares, O., Bucan, M., and Birnbaum, M.J. 2001. A role for AMP-activated protein kinase in contraction- and hypoxia-regulated glucose transport in skeletal muscle. *Mol. Cell.* **7**:1085–1094.

42. Stahmann, N., Woods, A., Carling, D., and Heller, R. 2006. Thrombin activates AMP-activated protein kinase in endothelial cells via a pathway involving Ca2+/calmodulin-dependent protein kinase kinase beta. *Mol. Cell. Biol.* **26**:5933–5945.

43. Rhee, S.G. 2006. Cell signaling. H2O2, a necessary evil for cell signaling. *Science.* **312**:1882–1883.

44. Ramirez, D.C., Mejiba, S.E., and Mason, R.P. 2005. Copper-catalyzed protein oxidation and its modulation by carbon dioxide: enhancement of protein radicals in cells. *J. Biol. Chem.* **280**:27402–27411.

45. Bertorello, A.M., and Sznajder, J.I. 2005. The dopamine paradox in lung and kidney epithelia: sharing the same target but operating different signaling networks. *Am. J. Respir. Cell Mol. Biol.* **33**:432–437.

46. Woods, A., et al. 2003. LKB1 is the upstream kinase in the AMP-activated protein kinase cascade. *Curr. Biol.* **13**:2004–2008.

47. Hawley, S.A., et al. 2005. Calmodulin-dependent protein kinase kinase-beta is an alternative upstream kinase for AMP-activated protein kinase. *Cell Metab.* **2**:9–19.

48. Woods, A., et al. 2005. Ca2+/calmodulin-dependent protein kinase kinase-beta acts upstream of AMP-activated protein kinase in mammalian cells. *Cell Metab.* **2**:21–33.

49. Hardie, D.G., Hawley, S.A., and Scott, J.W. 2006. AMP-activated protein kinase — development of the energy sensor concept. *J. Physiol.* **574**:7–15.

50. Hawley, S.A., et al. 2003. Complexes between the LKB1 tumor suppressor, STRAD alpha/beta and MO25 alpha/beta are upstream kinases in the AMP-activated protein kinase cascade. *J. Biol.* **2**:28.

51. Sakamoto, K., et al. 2006. Deficiency of LKB1 in heart prevents ischemia-mediated activation of AMPKalpha2 but not AMPKalpha1. *Am. J. Physiol. Endocrinol. Metab.* **290**:E780–E788.

52. Sanders, M.J., et al. 2007. Investigating the mechanism for AMP activation of the AMP-activated protein kinase cascade. *Biochem. J.* **403**:139–148.

53. Tamas, P., et al. 2006. Regulation of the energy sensor AMP-activated protein kinase by antigen receptor and Ca2+ in T lymphocytes. *J. Exp. Med.* **203**:1665–1670.

54. Rocher, A., et al. 2005. Role of voltage-dependent calcium channels in stimulus-secretion coupling in rabbit carotid body chemoreceptor cells. *J. Physiol.* **562**:407–420.

55. Filosa, J.A., and Putnam, R.W. 2003. Multiple targets of chemosensitive signaling in locus coeruleus neurons: role of K+ and Ca2+ channels. *Am. J. Physiol. Cell Physiol.* **284**:C145–C155.

56. Bootman, M.D., Lipp, P., and Berridge, M.J. 2001. The organisation and functions of local Ca2+ signals. *J. Cell Sci.* **114**:2213–2222.

57. Rizzuto, R., and Pozzan, T. 2006. Microdomains of intracellular Ca2+: molecular determinants and functional consequences. *Physiol. Rev.* **86**:369–408.

58. Berridge, M.J. 2006. Calcium microdomains: organization and function. *Cell Calcium.* **40**:405–412.

59. Marunaka, Y., Niisato, N., O'Brodovich, H., and Eaton, D.C. 1999. Regulation of an amiloride-sensitive Na+-permeable channel by a beta2-adrenergic agonist, cytosolic Ca2+ and Cl- in fetal rat alveolar epithelium. *J. Physiol.* **515**:669–683.

60. Marunaka, Y., Tohda, H., Hagiwara, N., and O'Brodovich, H. 1992. Cytosolic Ca2+-induced modulation of ion selectivity and amiloride sensitivity of a cation channel and beta agonist action in fetal lung epithelium. *Biochem. Biophys. Res. Commun.* **187**:648–656.

61. Vivona, M.L., Matthay, M., Chabaud, M.B., Friedlander, G., and Clerici, C. 2001. Hypoxia reduces alveolar epithelial sodium and fluid transport in rats: reversal by beta-adrenergic agonist treatment. *Am. J. Respir. Cell Mol. Biol.* **25**:554–561.

62. Planes, C., et al. 2002. Hypoxia and beta 2-agonists regulate cell surface expression of the epithelial sodium channel in native alveolar epithelial cells. *J. Biol. Chem.* **277**:47318–47324.

63. Wodopia, R., et al. 2000. Hypoxia decreases proteins involved in epithelial electrolyte transport in A549 cells and rat lung. *Am. J. Physiol. Lung Cell Mol Physiol.* **279**:L1110–L1119.

64. Ware, L.B., and Matthay, M.A. 2001. Alveolar fluid clearance is impaired in the majority of patients with acute lung injury and the acute respiratory distress syndrome. *Am. J. Respir. Crit. Care Med.* **163**:1376–1383.

65. Frank, J.A., et al. 2007. Physiological and biochemical markers of alveolar epithelial barrier dysfunction in perfused human lungs. *Am. J. Physiol. Lung Cell Mol. Physiol.* **293**:L52–L59.

66. McAuley, D., Frank, J., Fang, X., and Matthay, M. 2004. Clinically relevant concentrations of beta2-adrenergic agonists stimulate maximal cyclic adenosine monophosphate-dependent airspace fluid clearance and decrease pulmonary edema in experimental acid-induced lung injury. *Crit. Care Med.* **32**:1470–1476.

67. Azzam, Z.S., et al. 2001. Catecholamines increase lung edema clearance in rats with increased left atrial pressure. *J. Appl. Physiol.* **90**:1088–1094.

68. Saldias, F.J., et al. 2000. beta-adrenergic stimulation restores rat lung ability to clear edema in ventilator-associated lung injury. *Am. J. Respir. Crit. Care Med.* **162**:282–287.

69. Tokumitsu, H., et al. 2002. STO-609, a specific inhibitor of the Ca(2+)/calmodulin-dependent protein kinase kinase. *J. Biol. Chem.* **277**:15813–15818.

70. Hallows, K.R., Kobinger, G.P., Wilson, J.M., Witters, L.A., and Foskett, J.K. 2003. Physiological modulation of CFTR activity by AMP-activated protein kinase in polarized T84 cells. *Am. J. Physiol. Cell Physiol.* **284**:C1297–C1308.

71. Zou, M.H., et al. 2002. Modulation by peroxynitrite of Akt- and AMP-activated kinase-dependent Ser1179 phosphorylation of endothelial nitric oxide synthase. *J. Biol. Chem.* **277**:32552–32557.

72. Lecuona, E., Ridge, K., Pesce, L., Batlle, D., and Sznajder, J.I. 2003. The GTP-binding protein RhoA mediates Na,K-ATPase exocytosis in alveolar epithelial cells. *Mol. Biol. Cell.* **14**:3888–3897.

73. Lecuona, E., et al. 2006. Na,K-ATPase alpha1-subunit dephosphorylation by protein phosphatase 2A is necessary for its recruitment to the plasma membrane. *FASEB J.* **20**:2618–2620.

74. Ridge, K.M., et al. 2002. Dopamine-induced exocytosis of Na,K-ATPase is dependent on activation of protein kinase C-epsilon and -delta. *Mol. Biol. Cell.* **13**:1381–1389.

75. Rust, C., et al. 2000. The bile acid taurochenodeoxycholate activates a phosphatidylinositol 3-Kinase-dependent survival signaling cascade. *J. Biol. Chem.* **275**:20210–20216.